Journal of Power Sources 185 (2008) 857–861

Contents lists available at ScienceDirect

Journal of Power Sources

journal homepage: www.elsevier.com/locate/jpowsour

Short communication

Carbon supported platinum–gold alloy catalyst for direct formic acid fuel cells

J.B. Xu, T.S. Zhao*, Z.X. Liang

Department of Mechanical Engineering, The Hong Kong University of Science and Technology, Clear Water Bay, Kowloon, Hong Kong SAR, China

ARTICLE INFO

Article history:
Received 4 August 2008
Received in revised form
11 September 2008
Accepted 11 September 2008
Available online 20 September 2008

Keywords:
Direct formic acid fuel cells
Pt–Au alloy
Catalytic activity
Cell performance

ABSTRACT

The Pt–Au nanoparticles with 1:1 atomic ratio supported on carbon powder were prepared by the co-reduction method using *N*,*N*-dimethylformamide coordinated Pt–Au complex as a precursor. Cyclic voltammetry results demonstrated that the PtAu/C catalyst exhibited a higher activity for the formic acid oxidation reaction than did the commercial Pt/C catalyst, reflected by its lower onset potential and higher peak current. The fuel cell performance test at 60 °C showed that the direct formic acid fuel cell with the PtAu/C catalyst yielded about 35% higher power density than did the cell with the Pt/C catalyst.

1. Introduction

Liquid fuel-feed fuel cells, given their relatively simple system design and cell operation [1–3], are attractive as a power source for portable electronic devices. Among various liquid fuel-feed fuel cells, direct methanol fuel cells (DMFCs) have been extensively investigated and a significant progress has been made in the development of this type of fuel cell [4–7]. However, despite many years of intensive research into the DMFC technology, inherent limitations still remain. Methanol is toxic and sluggish in the anodic oxidation kinetics; moreover, DMFCs suffer from fuel crossover through Nafion-based membranes [2,8,9]. For these reasons, increasing attention has been paid to the search for alterative liquid fuels. Formic acid exhibits a smaller crossover flux through Nafion membrane than does methanol [10,11], allowing the use of high concentrated fuel solutions and thinner membranes in direct formic acid fuel cells (DFAFCs). DFAFCs also have a higher electromotive force, as calculated from the Gibbs free energy, than DMFCs [12]. In addition, formic acid is a strong electrolyte that facilitates proton transport in catalyst layers [13]. Although the theoretical energy density of formic acid (2086 Wh L^{-1}) is less than half of that of methanol (4690 Wh L^{-1}), the lower rate of fuel crossover through the Nafion-membrane allows higher fuel concentrations to be used than in the case of DMFCs. This is highly desirable for the design of compact portable power systems. In only a few years of research, the DFAFC technology has shown electrocatalytic oxidation activity far superior to DMFCs and, in some cases performance has approached that of H_2-PEM fuel cells [14]. Thus, for many systems, especially smaller power systems, the advantages of DFAFC can outweigh those of its primary direct-liquid fuel cell contender, the DMFC. Hopefully, DFAFC will become one of the earliest commercialized small power sources among low temperature fuel cells.

Platinum has been well known as the most effective catalyst for the formic acid oxidation, the mechanism of the formic acid elelctrooxidation on Pt and selected Pt-group metal surfaces in acid solution is the reasonably well-established, so-called dual pathway originally suggested by Capon and Parsons [15]:

$$\text{HCOOH} \xrightarrow{\text{dehydrogenation}} CO_2 + 2H^+ + 2e^- \quad (1)$$

$$\text{HCOOH} \xrightarrow{\text{dehydration}} CO_{ads} + H_2O \quad (2)$$

In this mechanism the direct path is normally a fast reaction involving an "active intermediate", while the second reaction proceeds via a "poisoning" intermediate, e.g. adsorbed carbon monoxide (CO_{ads}), which blocks the direct path. Numerous studies showed that the rate of poisoning depends strongly on the structural surface conditions of the electrode [16–18]. In practical applications, a modification of the Pt surface by some foreign atoms is required. The addition of foreign metals to Pt or more generally to metal electrode surfaces results in modified surface catalytic properties [19,20]. Therefore, bimetallic electrode surfaces often show an improved electrocatalytic behavior. A significant increase in the

* Corresponding author. Tel.: +852 2358 8647.
E-mail address: metzhao@ust.hk (T.S. Zhao).

0378-7753/$ – see front matter © 2008 Elsevier B.V. All rights reserved.
doi:10.1016/j.jpowsour.2008.09.039

rate of the formic acid oxidation was found on Pt–Ru, Pt–Bi and Pt–Au surfaces on the basis of a bifunctional mechanism, an electronic effect, or an ensemble effect [21–23]. Markovic and Ross [24] underlined that the formic acid oxidation was a reaction where the ensemble effect was very important. They observed a significant enhancement in the activity of the Pt surface by modification with either Ru or Sn and, reported that the very strong ensemble effect was observed on Ru- and Sn-modified surfaces. Pt–Au electrocatalyst has been reported as one of the best catalysts for formic acid oxidation reaction and its high activity is likely due to the so-called ensemble effect [25,26,13,27], which suggests that the addition of a second element to Pt reduces the CO adsorption and the surface poisoning effect is thus suppressed. For example, Choi et al. [13] found that the incorporation of Au could lead to the segregation of Pt sites and further reduce the number of adsorption sites for CO, thereby yielding an improvement in the activity of the formic acid oxidation. In summary, it is crucial to control the surface composition of the PtAu alloy catalysts to improve the catalytic activity of the formic acid oxidation.

The surface composition of the metal alloy nanoparticles is closely related to the preparation method used. Alloy nanoparticles can be conveniently synthesized by simultaneous reduction of two or more metal ions [28,29]. However, the synthesis of single-phase Pt–Au alloy nanoparticles is complicated due to the different reduction kinetics of Pt and Au ions [28] and the thermodynamic immiscibility [30]. Hence, the synthesis of Pt–Au alloy nanoparticles is a complex problem because of the composition control in addition to size and size distribution control. Another concern with the preparation of the bimetallic alloy, however, is whether the different metals will segregate either immediately upon contact with the support or under the conditions necessary to form an active catalyst.

In this work, we used the *N*,*N*-dimethylformamide (DMF) coordinated Pt–Au complex as the precursor for the synthesis of carbon supported Pt–Au alloy nannoparticles. This approach offers the potential of controlling the composition of the derived catalyst particles, allowing one to probe the role of the individual components in a bimetallic catalyst [31]. The prepared nanoparticles were characterized with TEM, EDS, XRD and XPS measurements. The alloy-dependent catalytic properties of the Pt–Au nanoparticles were characterized by cyclic voltammetry method through the formic acid electro-oxidation reaction. The DFAFC performance test showed that the PtAu/C nanocatalyst used at the anode of the fuel cell yielded higher performance than did the commercial E-TEK Pt/C catalyst.

2. Experimental

All of the chemicals used were of analytical grade. Hexachloroplatinic acid and hydrogen tetrachloroaurate trihydrate were purchased from Aldrich. *N*,*N*-dimethylformamide (DMF), ethanol, formic acid, sulfuric acid, sodium hydroxide and potassium chloride (all from Merk KGaA) were used as received. Vulcan XC-72 carbon (particle size 20–40 nm) and carbon supported Pt catalyst (30 wt%) were procured from E-TEK Company. 5 wt% Nafion solution was received from Dupont and used as received.

The preparation method of the catalyst is as follows: 20 mL of 10 mM H_2PtCl_6 and $HAuCl_4$ DMF solution were mixed and illuminated with UV light (250 nm, 300 W) for 3 h [31]. 182 mg of carbon powder was suspended into the resulting solution under vigorous stirring. After a homogeneous suspension was formed, 40 mL 0.2 M NaOH solution was added into the mixture under steady stirring at room temperature. The precipitate thus formed was collected by centrifugation, washed several times with ethanol and water and dried at 70 °C in oven (Pt–Au loading: 30 wt%, with platinum to gold mole ratio of 1:1).

Electrochemical measurements were carried out by cyclic voltammetry (CV) using a potentiostat (EG&G Princeton, model 273A). A conventional, three-electrode cell consisting of GCE with an area of 0.125 cm^2 as the working electrode, Pt foil as the counter electrode, and a saturated calomel electrode (SCE) as the reference electrode was used. The reference electrode was placed in a separate chamber, which was located near the working electrode through a Luggin capillary tube. The working electrode was modified with the catalyst layer achieved by dropping a suitable amount of catalyst ink on the GCE. The catalyst ink was prepared by ultrasonically dispersing 10 mg of 30 wt% of Pt/C and PtAu/C in 1.9 mL of ethanol, to which 0.1 mL of 5 wt% Nafion solution was added, and the dispersion was ultrasonicated for 30 min to obtain a homogeneous solution. A quantity of 6 μL of the dispersion was pipetted out on the top of the GCE and dried in air to yield a metal loading of 72 $\mu g\,cm^{-2}$. The CV experiments were performed in 0.5 M H_2SO_4 solution containing 0.5 M HCOOH at a scan rate of 50 $mV\,s^{-1}$. Solutions were prepared from analytical grade reagents and DI water. All experiments were done at room temperature in nitrogen (99.9%) saturated solutions.

The in-house fabricated DFAFC consisted of a membrane electrode assembly (MEA), with an active area of 2.3 cm × 2.3 cm, sandwiched between two bipolar plates, which were fixed by two fixture plates. The MEA consisted of a Nafion 115 membrane and two electrodes. For fabrication of the anode, commercial-grade 30 wt% Teflon-treated carbon paper (E-TEK) was employed as the backing layer. The gas diffusion layer (GDL) was fabricated on one side of the carbon paper comprising Vulcan XC-72 carbon and 30 wt% Teflon. To fabricate anode catalyst layers, the anode inks were prepared by mixing in-house-made 30 wt% PtAu/C and Pt/C with 10 wt% Nafion in ethanol. The prepared anode inks were uniformly brushed on the GDL in a 5.3 cm^2 area to give an approximate metal loading of 2.0 $mg\,cm^{-2}$ on the anode. Finally, 0.5 $mg\,cm^{-2}$ of Nafion was uniformly coated on the anode catalyst layers and dried at 80 °C in oven. The commercial Pt black (4 $mg\,cm^{-2}$) catalyst was used at the cathode. The MEA was formed by sandwiching the Nafion 115 membrane between the anode and the cathode and by hot pressing at 135 °C under a pressure of 4 MPa for 3 min.

The MEAs fabricated by using the PtAu/C and Pt/C catalysts at the anode were tested in a single cell fixture (with an active area of 5.29 cm^2) having three-pass serpentine flow channels with both widths and depths of 0.7 mm. The MEAs were initially activated at 60 °C for 24 h by feeding 2 M formic acid at a flow rate of 2 $mL\,min^{-1}$ to the anode and dry oxygen gas at a flow rate of 100 sccm to the cathode. After the activation process, the DFAFC performance curves were recorded by fixing the load current, which was controlled with an electric load system (BT2000, Arbin Instrument, Inc.).

3. Results and discussion

3.1. Physicochemical characterization of PtAu/C nanoparticles

Fig. 1 shows typical TEM images of the PtAu/C sample. It can be observed that Pt–Au alloy nanoparticles are well dispersed and do not aggregate with each other to form larger clusters, and are roughly in a spherical shape. From the high-resolution TEM (HRTEM) image shown in Fig. 1b, it can be seen that the Pt–Au nanoparticles appear to be entirely crystalline, as evidenced by the lattice fringes across the full extent of image. Fig. 2 shows the distribution of particle diameter estimated from an ensemble of 150 particles in an arbitrarily chosen area of the HRTEM images. The evaluation of the characteristic diameter of the Pt–Au particles indi-

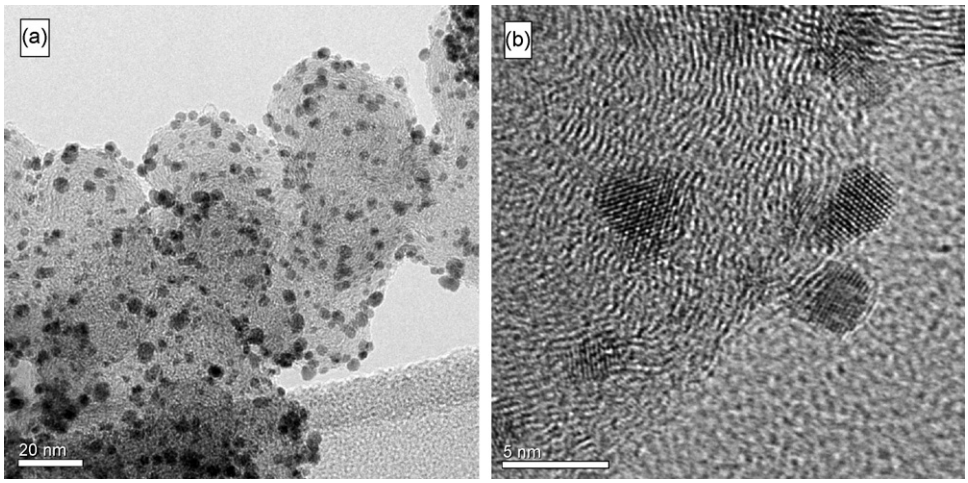

Fig. 1. TEM (a) and HRTEM (b) images of the PtAu/C.

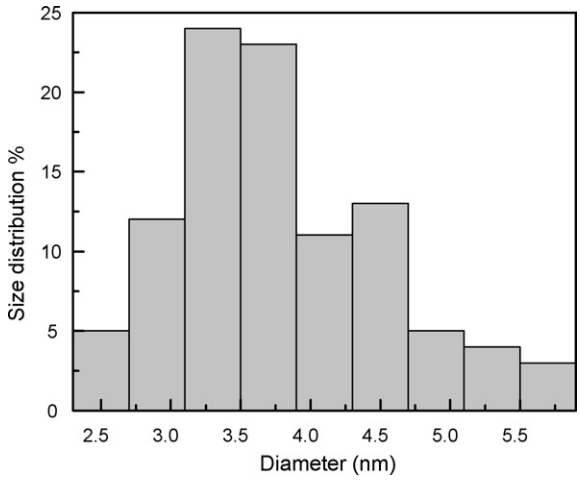

Fig. 2. Histogram of Pt–Au particle size distribution.

cates a size distribution from 2.4 to 5.8 nm with an average diameter of 3.8 nm. The composition of Pt–Au particles analyzed by EDS is shown in Fig. 3. It has an elemental composition of 50.6 at% Pt and 49.4 at% Au, which is consistent with the Pt:Au ratio in the precursor (with platinum to gold mole ratio of 1:1).

In order to obtain the information of the average particle size and the Pt–Au alloy effect, the PtAu/C sample was characterized by XRD and is shown in Fig. 4 alongside the diffraction pattern of the Pt/C catalyst used as comparison. The pattern of the PtAu/C exhibited diffraction peaks of (1 1 1), (2 0 0), (2 2 0), and (3 1 1) at 2θ values of 38.75°, 44.43°, 65.42°, and 79.07°, respectively. These peaks indicate that Pt is present in the face-centered cubic (fcc) structure [32]. Compared to that of the Pt/C, the shift of the (1 1 1) peak to a lower 2θ angle by about 0.85° could be indexed to a higher d space (d_{111} = 2.322 Å) crystal structure of Pt as a result of the incorporation of the Au atoms, indicating that the single phase Pt–Au alloy was formed on the carbon powder [33]. The average particle size of PtAu/C catalysts was 3.0 nm, calculated from the broadening of the (2 2 0) diffraction peaks using Scherrer's equation [34]:

$$d = \frac{0.9\lambda}{B_{2\theta}\ \cos\theta_{\max}} \tag{3}$$

where λ is the wavelength of the X-ray (1.54056 Å), θ is the angle at the maximum of the peak, and $B_{2\theta}$ is the width of the peak at half-height.

XPS was employed to analyze the valence state and the surface composition of the carbon supported particles. Fig. 5 shows the regional Pt4f and Au4f spectra of the PtAu/C sample. The peaks at 71.4 and 74.7 eV can be assigned to Pt^0, while the peaks at 84.0 and 87.7 eV correspond to Au^0 [35,36]. Furthermore, on the basis of the intensities of the XPS peaks, the elemental composition of the

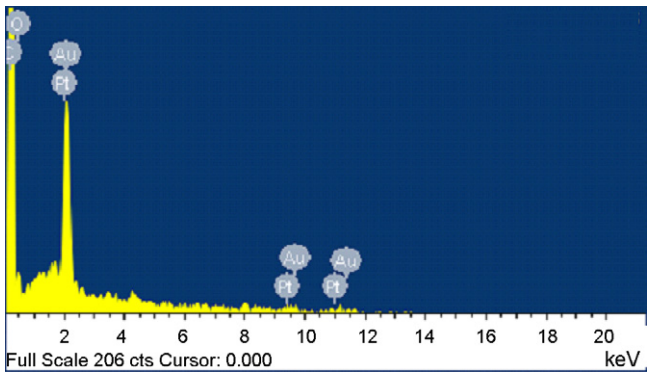

Fig. 3. EDS spectrum of the PtAu/C particles.

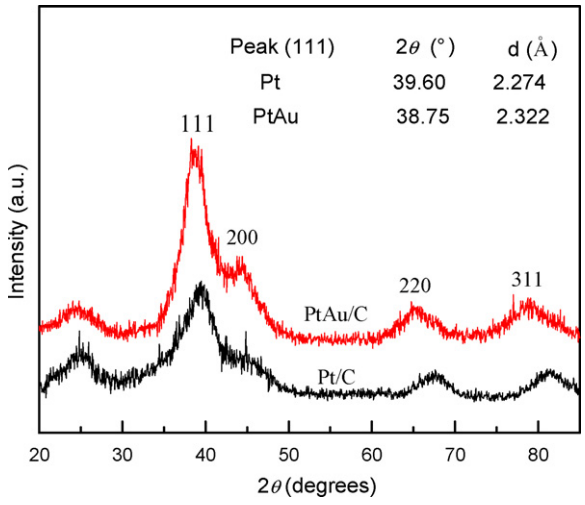

Fig. 4. XRD pattern of the PtAu/C and Pt/C samples.

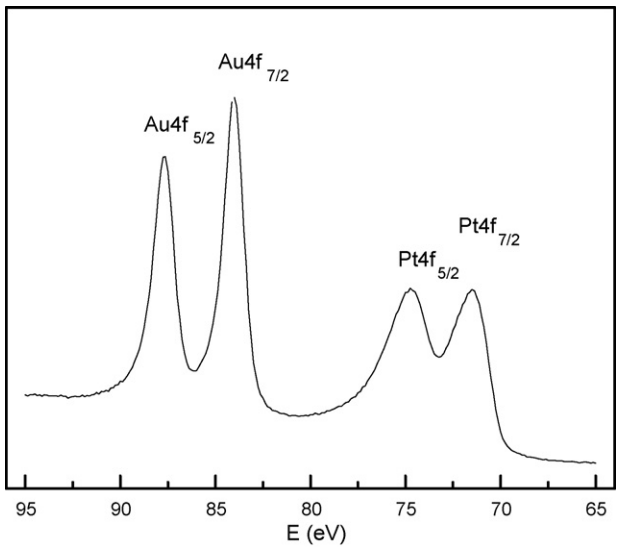

Fig. 5. XPS spectrum of the PtAu/C sample.

bimetallic nanoparticles could be obtained with the surface atomic ratio of Pt:Au is 1.04:1 which agrees well with the EDS analysis.

3.2. Electrochemical characterization of the PtAu/C catalyst

Fig. 6 compares the typical CV curves of the PtAu/C and Pt/C catalysts measured in 0.5 M H_2SO_4 + 0.5 M HCOOH in the potential range between −0.2 and 0.6 V, which is the typical potential region for the operation of formic acid fuel cells. As can be seen in Fig. 6 (the 40th circle), during the positive-going scan, the current increases rapidly until a current peak is seen at ca. 0.30 V. As to the negative-going scan, another anodic peak is observed at approximately the same potential as the first anodic peak on both electrodes. This peak at around 0.30 V is related to the direct oxidation of HCOOH to form CO_2 [25]. Even though the general features of the voltammetric curves are somewhat similar, it is evident that the electrode composition has a significant influence on the behavior toward formic acid oxidation. The onset potential is about −0.09 V for PtAu/C catalyst, but ca. 0 V for Pt/C, which shifted to a much lower potential. The lower onset potential of the anodic peak in the forward scan indicates that the PtAu/C catalyst has a superior catalytic activity toward the formic acid electrooxidation

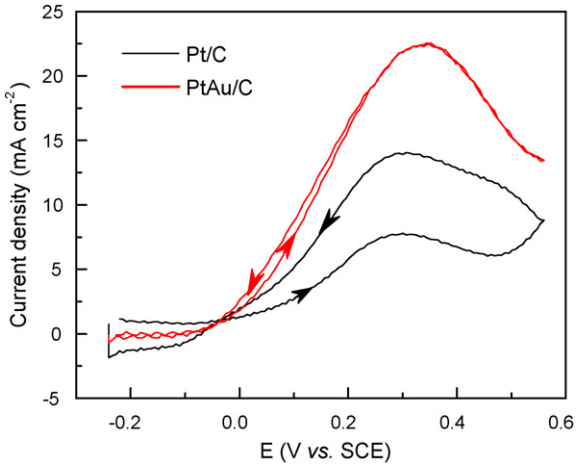

Fig. 6. CV curves in 0.5 M H_2SO_4 + 0.5 M HCOOH at 50 mV/s.

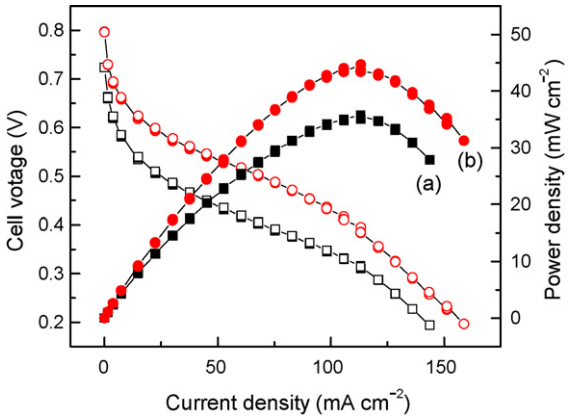

Fig. 7. Single cell performance of Pt/C (a) and PtAu/C (b) anode and Pt cathode. Cell temperature: 60 °C. Formic acid: 2 ml min^{-1}, 2 M. Oxygen: 100 sccm.

reaction. Moreover, The enhanced electrocatalytic activity for the formic acid oxidation reaction with PtAu/C can be clearly reflected by the higher current density and the lack of hysteresis. The significant improvement can be attributed to the addition of Au, which leads to a high utilization of Pt due to the ensemble effect [25,26,13]. It was reported that the noncontinuous Pt sites favor the dehydrogenation process in the presence of the neighbored Pt and Au sites. And we assume that the unique behavior of the Pt–Au alloy for formic acid oxidation reaction could increase cell potential/power density during the operation of DFAFCs.

3.3. Direct formic acid fuel cell performance test

Fig. 7 shows polarization and power density curves of the DFAFC using the 30 wt% PtAu/C and the commercial Pt/C (E-TEK) as the anode catalyst with 2 M formic acid at 60 °C. It can be observed that the open-circuit voltage (OCV) is strongly dependent on the composition of the catalyst. With the Pt/C catalyst at the anode, the OCV is about 0.72 V, which is 0.08 V lower than that with the PtAu/C (ca. 0.80 V). This is consistent with the earlier discussion on the onset potential of formic acid oxidation in CV characterizations. Also, it can be seen that the PtAu/C at the anode yielded a maximum power density of 44 mW cm^{-2}, whereas the Pt/C catalyst gave a maximum power density of around 35 mW cm^{-2} under the same operating conditions of DFAFCs. Therefore, the results confirm that the synthesized PtAu/C catalyst exhibits a higher catalytic activity for the formic acid oxidation reaction than does the Pt/C catalyst. The higher electro-catalytic performance of the PtAu/C results from the reduced CO_{ads}-poisoning of Pt catalyst conferred by the addition of Au [18,13,27].

In order to investigate the concentration effect of the formic acid on the cell performance, a modest high concentration of formic acid was adopted to test the cell performance of the DFAFC [37]. Fig. 8 shows polarization and power density curves for the DFAFC using the PtAu/C and Pt/C as the anode and Pt cathode with 6 M formic acid at 60 °C. It can be observed that the OCV is dependent on the formic acid concentration. Using formic acid of 2.0 M, OCV is 0.72 V and it decreases to 0.65 V at 6.0 M for the Pt/C, 0.80 to 0.75 V for PtAu/C, respectively. The OCV is strongly dependent on the rate of fuel crossover, as formic acid is electrochemically oxidized at the cathode and therefore induces cathodic overpotential. A higher formic acid concentration at the anode yields more significant formic acid crossover, and hence the OCV declines with the increase in the fuel concentration. Furthermore, the maximum power density of the DFAFC is about 42 mW cm^{-2} for Pt/C and 64 mW cm^{-2} for PtAu/C, respectively. Based on the experimental

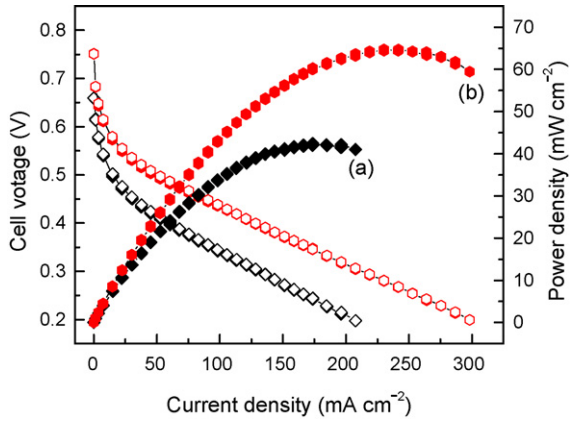

Fig. 8. Single cell performance of Pt/C (a) and PtAu/C (b) anode and Pt cathode. Cell temperature: 60 °C. Formic acid: 2 ml min^{-1}, 6 M. Oxygen: 100 sccm.

results, it can be observed that the DFAFC with PtAu/C (Pt loading: 1.0 mg cm^{-2}) as the anode catalyst yielded about 35% higher power densities than that of the Pt/C (Pt loading: 2.0 mg cm^{-2}) in 6 M formic acid, which makes the PtAu/C a more attractive anode catalyst in DFAFCs.

4. Conclusions

In conclusion, we demonstrated that bimetallic Pt–Au alloy nanoparticles supported on carbon powder were successfully prepared by the co-reduction method in DMF. The XRD analysis confirmed the formation of single phase Pt–Au alloy nanoparticles on the carbon powder. The TEM, EDS and XPS results indicated that well-dispersed Pt–Au particles with a controlled composition (1:1) were formed on the carbon support. The alloy-dependent catalytic properties of the PtAu/C alloy nanoparticles were analyzed by the CV method through the formic acid electro-oxidation reaction. The result demonstrated that the PtAu/C synthesized by this method exhibited higher catalytic activity than did the commercial Pt/C catalyst by giving lower onset potential and higher peak current for formic acid oxidation reaction. It was suggested that such an improvement results from the reduced CO-poisoning of Pt catalyst conferred by the neighboring Au atoms in the well-alloyed bimetallic catalyst. Furthermore, the performance tests of the direct formic acid fuel cells indicated the PtAu/C alloy catalyst synthesized using the method in this work is a promising catalyst for the electro-oxidation of formic acid.

Acknowledgement

The work described in this paper was fully supported by a grant from the Research Grants Council of the Hong Kong Special Administrative Region, China (Project No. 622807).

References

[1] C. Lamy, A. Lima, V. LeRhun, F. Delime, C. Coutanceau, J.M. Leger, J. Power Sources 105 (2002) 283.
[2] X.W. Yu, P.G. Pickup, J. Power Sources 182 (2008) 124.
[3] S.K. Kamarudin, W.R.W. Daud, S.L. Ho, U.A. Hasran, J. Power Sources 163 (2007) 743.
[4] R. Chen, T.S. Zhao, J. Power Sources 167 (2007) 455.
[5] C. Xu, T.S. Zhao, Electrochem. Commun. 9 (2007) 493.
[6] H.S. Liu, C.J. Song, L. Zhang, J.J. Zhang, H.J. Wang, D.P. Wilkinson, J. Power Sources 155 (2006) 95.
[7] W.W. Yang, T.S. Zhao, J. Power Sources 174 (2007) 136.
[8] G. Apanel, Fuel Cells Bull. (2004) 12.
[9] U.B. Demirci, J. Power Sources 173 (2007) 11.
[10] Y.W. Rhee, S.Y. Ha, R.I. Masel, J. Power Sources 117 (2003) 35.
[11] X. Wang, J.M. Hu, I.M. Hsing, J. Electroanal. Chem. 562 (2004) 73.
[12] U.B. Demirci, J. Power Sources 169 (2007) 239.
[13] J.H. Choi, K.J. Jeong, Y. Dong, J. Han, T.H. Lim, J.S. Lee, Y.E. Sung, J. Power Sources 163 (2006) 71.
[14] Y.M. Zhu, Z. Khan, R.I. Masel, J. Power Sources 139 (2005) 15.
[15] A. Capon, R. Parsons, J. Electroanal. Chem. 45 (1973) 205.
[16] S.L. Gojkovic, A.V. Tripkovic, R.M. Stevanovic, N.V. Krstajic, Langmuir 23 (2007) 12760.
[17] T.J. Schmidt, R.J. Behm, Langmuir 16 (2000) 8159.
[18] J.K. Lee, J. Lee, J. Han, T.H. Lim, Y.E. Sung, Y. Tak, Electrochim. Acta 53 (2008) 3474.
[19] H. Lee, S.E. Habas, G.A. Somorjai, P. Yang, J. Am. Chem. Soc. 130 (2008) 5406.
[20] S.Y. Uhm, S.T. Chung, J.Y. Lee, Electrochem. Commun. 9 (2007) 2027.
[21] N.M. Markovic, H.A. Gasteiger, P.N. Ross Jr., X. Jiang, I. Villegas, M.J. Weaver, Electrochim. Acta 40 (1995) 91.
[22] J. Clavilier, A. Fernandez-Vega, J.M. Feliu, A. Aldaz, J. Electroanal. Chem. 258 (1989) 89.
[23] E. Rach, J. Heitbaum, Electrochim. Acta 32 (1987) 1173.
[24] N.M. Markovic, P.N. Ross Jr., Surf. Sci. Rep. 45 (2002) 117.
[25] N. Kristian, Y.S. Yan, X. Wang, Chem. Commun. (2008) 353.
[26] S. Park, Y. Xie, M.J. Weaver, Langmuir 18 (2002) 5792.
[27] V. Ponec, Surf. Sci. 80 (1979) 352.
[28] L.M. Liz-Marzan, A.P. Philipse, J. Phys. Chem. 99 (1995) 15120.
[29] M.P. Mallin, C.J. Murphy, Nano Lett. 2 (2002) 1235.
[30] M.M. Mariscal, S.A. Dassie, E.P.M. Leiva, J. Chem. Phys. 123 (2005) 184505.
[31] J.B. Xu, T.S. Zhao, Z.X. Liang, L.D. Zhu, Chem. Mater. 20 (2008) 1688.
[32] J.B. Xu, K.F. Hua, G.Z. Sun, C. Wang, X.Y. Lv, Y.J. Wang, Electrochem. Commun. 8 (2006) 982.
[33] J. Luo, M.M. Maye, V. Petkov, N.N. Kariuki, L.Y. Wang, P. Njoki, D. Mott, Y. Lin, C.J. Zhong, Chem. Mater. 17 (2005) 3086.
[34] Z.X. Liang, T.S. Zhao, J. Phys. Chem. C 111 (2007) 8128.
[35] D.J. Davis, G. Kyriakou, R.M. Lambert, J. Phys. Chem. B 110 (2006) 11958.
[36] M.L. Wu, D.H. Chen, T.C. Huang, Chem. Mater. 13 (2001) 599.
[37] J. Yeom, R.S. Jayashree, C. Rastogi, M.A. Shannon, P.J.A. Kenis, J. Power Sources 160 (2006) 1058.